FISEVIER

Contents lists available at ScienceDirect

Journal of Computational and Applied Mathematics

journal homepage: www.elsevier.com/locate/cam





Weak Galerkin methods for elliptic interface problems on curved polygonal partitions

Dan Li ^{a,1}, Chunmei Wang ^{b,2,*}, Shangyou Zhang ^c

- ^a Jiangsu Key Laboratory for NSLSCS, School of Mathematical Sciences, Nanjing Normal University, Nanjing, 210023, China
- ^b Department of Mathematics, University of Florida, Gainesville, FL 32611, United States of America
- ^c Department of Mathematical Sciences, University of Delaware, Newark, DE 19716, United States of America

ARTICLE INFO

Keywords: Weak Galerkin Finite element methods Elliptic interface problems Weak gradient Polygonal partitions Curved elements

ABSTRACT

This paper presents a new weak Galerkin (WG) method for elliptic interface problems on general curved polygonal partitions. The method's key innovation lies in its ability to transform the complex interface jump condition into a more manageable Dirichlet boundary condition, simplifying the theoretical analysis significantly. The numerical scheme is designed by using locally constructed weak gradient on the curved polygonal partitions. We establish error estimates of optimal order for the numerical approximation in both discrete H^1 and L^2 norms. Additionally, we present various numerical results that serve to illustrate the robust numerical performance of the proposed WG interface method.

1. Introduction

This paper focuses on the latest advancements in the weak Galerkin finite element method for solving elliptic interface problems on curved polygonal partitions. To simplify our analysis, we concentrate on a model equation seeking an unknown function u that satisfies:

$$-\nabla \cdot (a\nabla u) = f, \quad \text{in } \Omega, \tag{1.1}$$

$$u = g, \quad \text{on } \partial\Omega \setminus \Gamma,$$
 (1.2)

$$[[u]]_{\Gamma} = u|_{\Omega_1} - u|_{\Omega_2} = g_D, \quad \text{on } \Gamma, \tag{1.3}$$

$$[[a\nabla u \cdot \mathbf{n}]]_{\Gamma} = a_1 \nabla u|_{\Omega_1} \cdot \mathbf{n}_1 + a_2 \nabla u|_{\Omega_2} \cdot \mathbf{n}_2 = g_N, \quad \text{on } \Gamma,$$

$$(1.4)$$

where $\Omega \subset \mathbb{R}^2$, $\Omega = \Omega_1 \cup \Omega_2$, $\Gamma = \Omega_1 \cap \Omega_2$, $a_1 = a|_{\Omega_1}$, $a_2 = a|_{\Omega_2}$, \mathbf{n}_1 and \mathbf{n}_2 represent the unit outward normal vectors to $\Omega_1 \cap \Gamma$ and $\Omega_2 \cap \Gamma$, respectively. Assume the diffusion tensor a is symmetric and uniformly positive definite matrix in Ω .

A weak formulation of the model Eqs. (1.1)–(1.4) is as follows: Find $u \in H^1(\Omega)$, such that u = g on $\partial \Omega \setminus \Gamma$, $[[u]]_{\Gamma} = g_D$ on Γ , satisfies

$$(a\nabla u, \nabla v) = (f, v) + \langle g_N, v \rangle_{\Gamma}, \quad \forall v \in H_0^1(\Omega),$$

$$(1.5)$$

E-mail addresses: danlimath@163.com (D. Li), chunmei.wang@ufl.edu (C. Wang), szhang@udel.edu (S. Zhang).

https://doi.org/10.1016/j.cam.2024.115995

Received 10 October 2023; Received in revised form 31 January 2024

Available online 11 May 2024

0377-0427/© 2024 Elsevier B.V. All rights are reserved, including those for text and data mining, AI training, and similar technologies.

^{*} Corresponding author.

¹ The research of Dan Li was supported by Jiangsu Funding Program for Excellent Postdoctoral Talent (Grant No. 2023ZB271), China Postdoctoral Science Foundation (Grant No. 2023M741763), National Postdoctoral Researcher Program (Grant No. GZB20230311), National Natural Science Foundation of China (Grants No. 12071227 and No. 12371369), and National Key Research and Development Program of China (Grant No. 2020YFA0713803).

² The research of Chunmei Wang was partially supported by National Science Foundation Grants DMS-2136380.

where $H_0^1(\Omega) = \{v \in H^1(\Omega), v = 0 \text{ on } \partial\Omega\}.$

Elliptic interface problems find applications in various fields of engineering and science, including biological systems [1], material science [2], fluid dynamics [3], computational electromagnetic [4,5]. The presence of a discontinuous diffusion tensor in these problems results in solutions that exhibit discontinuities and/or lack smoothness across the interface. This low regularity of the solution presents a significant challenge in the development of high-order numerical methods. To address the mesh constraints associated with interface problems effectively, researchers have proposed several numerical techniques. These methods include interface-fitted mesh approaches, which involve modifying finite element meshes near the interface, and unfitted mesh methods, which alter the finite element discretization around the interface.

Unfitted mesh methods have garnered significant attention for their ability to utilize finite element meshes independently of the interface. They offer two primary strategies for handling interface elements. One approach involves adapting the finite element basis near the interface to construct a finite element space that satisfies the interface jump condition. This strategy encompasses methods like the immersed interface method [6–9], ghost fluid methods [10], multiscale finite element methods [11], hybridizable discontinuous Galerkin methods [12,13]. Alternatively, another approach employs penalty terms across the interface to enforce the interface jump condition. This category includes methods like extended finite element methods [14,15], unfitted finite element methods [16], cut finite element methods [17], high-order hybridizable discontinuous Galerkin method [18]. Despite the successes achieved by unfitted mesh methods, several challenges remain. In particular, accurately capturing interface information for problems with highly complex interface geometries poses difficulties. Additionally, establishing rigorous convergence analyses for high-order numerical methods remains a challenging task.

As an alternative approach, several interface-fitted mesh methods have been developed to tackle elliptic interface problems. These methods aim to accommodate poorly generated meshes and situations with hanging nodes, particularly in the context of complex interfaces. Some notable methods include the discontinuous Galerkin method [18–20], the matched interface and boundary method [21,22], virtual element method [23] and weak Galerkin methods [24–27]. The WG methods, first introduced in [28] and further developed in [29–36] represent a novel class of numerical techniques for solving partial differential equations. Their primary innovation lies in the introduction of weak differential operators and weak functions, which grant WG methods several advantages. Notably, constructing high-order WG approximating functions becomes straightforward, as the continuity requirements for numerical approximations are relaxed. Furthermore, this relaxation of continuity requirements endows WG methods with high flexibility, particularly on general polygonal meshes with straight edges. However, when employing straight-edge elements to discretize regions with curved boundaries, high-order numerical methods may suffer from reduced accuracy. To mitigate geometric errors arising from the transition between straight-edge and curved-edge regions, one approach is to directly utilize curved-edge elements for discretizing curved geometries [37,38].

The objective of this paper is to introduce a novel weak Galerkin method designed for solving elliptic interface problems on general curved polygonal partitions. The new WG method is designed by using a locally constructed weak gradient operator on the curved elements. Moreover, the error estimates of optimal order are established for the high order numerical approximation in discrete H^1 norm and usual L^2 norms. What sets our approach apart from existing results on standard weak Galerkin methods is that it does not necessitate locally denser meshes near the interface. As a result, our proposed method not only significantly reduces the storage space and computational complexity but also offers greater flexibility in addressing complex interface geometries.

The remainder of the paper is structured as follows: In Section 2, we provide a concise overview of the computation of the weak gradient operator and its discrete counterpart. Section 3 outlines the application of the weak Galerkin method to solve the model problem described by Eqs. (1.1) through (1.4), based on the weak formulation presented in Eq. (1.5). Section 4 derives an error equation relevant to the weak Galerkin algorithm. Section 6 is focused on establishing error estimates of optimal order for the corresponding numerical approximations, considering both discrete H^1 and conventional L^2 norms. Finally, in Section 7, we illustrate the practical application of the theoretical results through several numerical examples.

This paper will adhere to the standard notations for Sobolev spaces and norms, as detailed in [39]. Let D be an open bounded domain with a Lipschitz continuous boundary denoted as ∂D in \mathbb{R}^2 . We employ the symbols $(\cdot, \cdot)s$, D, $|\cdot|s$, D, and $||\cdot||s$, D to represent the inner product, seminorm, and norm within the Sobolev space D is an integer. In the case of D in the corresponding inner product and norm as D in the sake of simplicity, we use the notation "D in the corresponding inner product and norm notations. For the sake of simplicity, we use the notation "D in the corresponding inner product and norm notations. For the sake of simplicity, we use the notation "D in the corresponding inner product and norm notations. For the sake of simplicity, we use the notation "D in the inequality "D in the inequalities.

2. Weak gradient and discrete weak gradient

The objective of this section is to provide a review of the definitions for the weak gradient operator and its discrete counterpart, as outlined in [28,40]. To facilitate this review, consider a polygonal domain T with a boundary ∂T that is Lipschitz continuous.

In this context, a weak function defined on T is represented as $v = \{v_0, v_b\}$, where $v_0 \in L^2(T)$ and $v_b \in L^2(\partial T)$. The first component v_0 and the second component v_b correspond to the values of v within the interior of T and on the boundary of T, respectively. It is worth noting that v_b may not necessarily be the trace of v_0 on ∂T .

Let W(T) be the space encompassing all such weak functions on T:

$$\mathcal{W}(T) = \{v = \{v_0, v_b\}, \ v_0 \in L^2(T), \ v_b \in L^2(\partial T)\}.$$

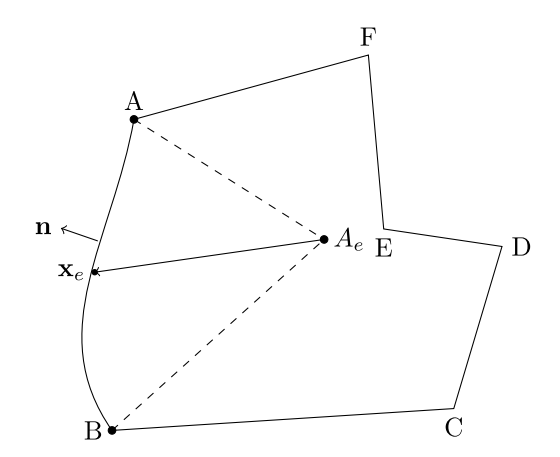


Fig. 3.1. Depiction of a shape-regular polygonal element ABCDEFA.

Definition 2.1 (Weak Gradient). For any $v \in \mathcal{W}(T)$, the weak gradient of v, denoted as $\nabla_w v$, is defined as a linear functional in the dual space of $[H^1(T)]^2$ such that

$$(\nabla_w v, \psi)_T = -(v_0, \nabla \cdot \psi)_T + \langle v_b, \psi \cdot \mathbf{n} \rangle_{\partial T}, \quad \forall \psi \in [H^1(T)]^2, \tag{2.1}$$

where **n** denotes the unit outward normal vector to ∂T .

For any non-negative integer r, we denote by $P_r(T)$ the set of polynomials defined on the polygonal domain T with a degree not exceeding r.

Definition 2.2 (Discrete Weak Gradient). A discrete form of $\nabla_w v$ for $v \in \mathcal{W}(T)$, denoted by $\nabla_{w,r,T} v$, is defined as a unique polynomial vector in $[P_r(T)]^2$ satisfying

$$(\nabla_{w,r,T}v, \boldsymbol{\psi})_T = -(v_0, \nabla \cdot \boldsymbol{\psi})_T + \langle v_b, \boldsymbol{\psi} \cdot \mathbf{n} \rangle_{\partial T}, \quad \forall \boldsymbol{\psi} \in [P_r(T)]^2. \tag{2.2}$$

3. Weak Galerkin scheme

In this section, we present the weak Galerkin scheme for the model problems described by Eqs. (1.1) through (1.4). Let \mathcal{T}_h be a curved finite element partition of Ω consisting of curved elements which are closed and not necessarily simply connected polygons; see Fig. 3.1. We denote \mathcal{E}_h as the set encompassing all edges within \mathcal{T}_h , and \mathcal{E}_h^0 as the set of all interior edges, excluding those along $\partial\Omega$. Additionally, Γ_h is defined as the set of interface edges within \mathcal{E}_h . h_T represents the diameter of an element $T \in \mathcal{T}_h$, and h is the meshsize, defined as the maximum of h_T over all $T \in \mathcal{T}_h$, respectively. Lastly, |e| denotes the length of an edge $e \in \mathcal{E}_h$. The curved finite element partition \mathcal{T}_h is said to be shape regular if the following conditions (A1)–(A4) are satisfied [41].

A1: For each element $T \in \mathcal{T}_h$, there exists a positive constant ϱ_v such that

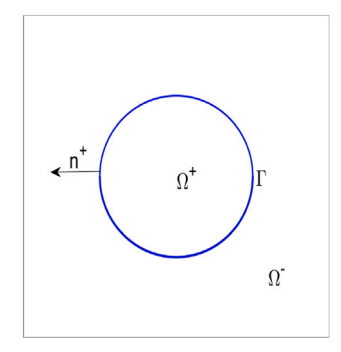
$$\varrho_v h_T^2 \le |T|$$
.

A2: For each element $T \in \mathcal{T}_h$, there exist positive constants κ and κ^* such that

$$\kappa h_T \leq h_o \leq \kappa^* h_T$$

for each edge $e \subset \partial T$.

- A3: For each element $T \in \mathcal{T}_h$ and each edge $e \subset \partial T$, there exists a "pyramid" $P(e,T,A_e)$ contained in T such that its curved base is identical with e, its apex is $A_e \in T$, and its height is proportional to h_T with a proportionality constant σ_e bounded by a fixed positive number σ^* from below. In other words, the height of the "pyramid" is given by $\sigma_e h_T$ such that $\sigma_e \geq \sigma^* > 0$. The "pyramid" is also assumed to stand up above the curved base e in the sense that the angle between the vector $\overline{A_e x_e}$, for any $x_e \in e$, and the outward normal direction of e (i.e., the vector \mathbf{n} in Fig. 3.1) is strictly acute by falling into an interval $[0,\theta_0]$ with $\theta_0 < \frac{\pi}{2}$.
- A4: For each element $T \in \mathcal{T}_h$, there is a triangle S(T) circumscribing T that is shape regular and the diameter of S(T), denoted by $h_{S(T)}$, is proportional to the diameter of T; i.e., $h_{S(T)} \leq \gamma_* h_T$ with a constant γ_* independent of T. Furthermore, assume that each circumscribing triangle S(T) intersects with only a fixed and small number of such triangles for all other elements $T \in \mathcal{T}_h$.



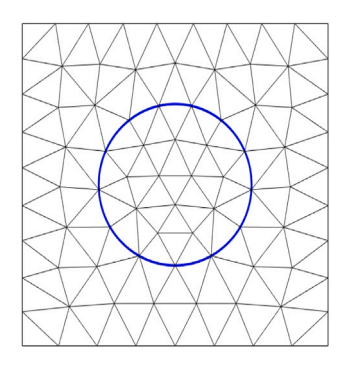


Fig. 3.2. The geometry of domain $\Omega = \Omega_1 \cup \Omega_2 \cup \Gamma$ with smooth interface Γ (Left) and a fitted partition (Right).

For the sake of simplicity, Fig. 3.2 displays a curved triangular partition of a square domain, denoted as Ω . It is worth noting that when the interface Γ is curved, \mathcal{T}_h fits seamlessly along the interface.

Let e be the curved edge of the curved element T. Suppose that the parametric representation for edge e is given by:

$$\mathbf{x} = F_{e}(\hat{t}), \qquad \hat{t} \in \hat{e} = [0, |e|],$$

where $\mathbf{x}=(x,y)\in e$, $F_e(\hat{t})=(\phi(\hat{t}),\psi(\hat{t}))$, $\phi(\hat{t})\in C^n(\hat{e})$, $\psi(\hat{t})\in C^n(\hat{e})$ for some $n\geq 1$. In this context, $F_e:=(\phi,\psi)$ represents the mapping that transforms the curved edge e to its corresponding straight edge \hat{e} , and we assume that this mapping F_e is globally invertible on the reference edge \hat{e} . Then, F_e and its inverse mapping $\hat{F}_e:=F_e^{-1}$ can be extended to encompass the entire "pyramid" region, as discussed in [41].

For any function $\hat{w} \in L^2(\hat{e})$, we can use the mapping \hat{F}_e to obtain a function $w \in L^2(e)$ as follows:

$$w(\mathbf{x}) := \hat{w}(\hat{F}_e(\mathbf{x})), \quad \mathbf{x} \in e.$$
 (3.1)

Similarly, any function $w \in L^2(e)$ can be transformed into a function $\hat{w} \in L^2(\hat{e})$ given by

$$\widehat{w}(\widehat{t}) := w(F_e(\widehat{t})), \quad \widehat{t} \in \widehat{e}. \tag{3.2}$$

Consequently, we have the relationships:

$$w = \hat{w} \circ \hat{F}_{e}, \quad \hat{w} = w \circ F_{e}.$$

Let $\ell \geq 0$ be any non-negative integer. We denote by $P_{\ell}(\hat{e})$ the set of polynomials defined on the straight edge \hat{e} with a degree no greater than ℓ . By utilizing the mapping $\hat{F}_e := F_e^{-1}$, we can transform the set of polynomials $P_{\ell}(\hat{e})$ into a space of functions defined on the curved edge e. This transformed space is denoted as follows:

$$V_b(e,\ell) = \{ w = \hat{w} \circ \hat{F}_e : \hat{w} \in P_\ell(\hat{e}) \}.$$

Moreover, when the edge e is a straight edge, we make the assumption that the mapping F_e is an affine transformation. Consequently, the inverse mapping \hat{F}_e is also an affine transformation. In this special case, it follows that

$$V_b(e, \ell) = P_{\ell}(e).$$

Let $k \ge 1$ be any given integer. Denote by $V_k(T)$ the local discrete weak finite element space on T given by

$$V_k(T) = \{ v = \{ v_0, v_h \} : v_0 \in P_k(T), v_h |_e \in V_h(e, k-1), e \in \partial T \}.$$

By patching $V_k(T)$ over all the elements $T \in \mathcal{T}_h$ through a common value v_b on each interior edge in $\mathcal{E}_h^0 \setminus \Gamma_h$, we arrive at a global weak finite element space V_h :

$$V_h = \{ v = \{ v_0, v_b \} : v|_T \in V_k(T), \ v_b \text{ is single-valued on } \mathcal{E}_h \setminus \Gamma_h,$$

$$v_b|_{T_k \cap e} \neq v_b|_{T_k \cap e}, e \in \Gamma_h \},$$

$$(3.3)$$

where the edge $e \in \Gamma_h$ is shared by two adjacent elements $T_L \subset \Omega_1$ and $T_R \subset \Omega_2$, $v_b|_{T_L \cap e}$ and $v_b|_{T_R \cap e}$ represent the values of v on the edge $e \in \Gamma_h$ as seen from the left element T_L and from the right element T_R , respectively.

Denote by V_h^0 a subspace of V_h with homogeneous boundary value for v_b ; i.e.,

$$V_h^0 = \{ v \in V_h, \ v_h|_e = 0, \ e \subset \partial \Omega \}.$$

For simplicity of notation, denote by $\nabla_w v$ the discrete weak gradient $\nabla_{w,r,T} v$ defined by (2.2) on each element T with r = k - 1; i.e.,

$$(\nabla_w v)|_T = \nabla_{w,r,T}(v|_T), \qquad v \in V_h. \tag{3.4}$$

For each edge $e \in \mathcal{E}_h$, denote by Q_h the projection operator mapping from $L^2(e)$ to $V_h(e,k-1)$ given by

$$Q_b w \circ F_e := \widehat{Q}_b(w \circ F_e), \qquad w \in L^2(e),$$

where \hat{Q}_b is the weighted L^2 projection operator onto $P_{k-1}(\hat{e})$ with the corresponding Jacobian as the weight function. Note that when e is a straight edge, the operator Q_b represents the standard L^2 projection operator onto $P_{k-1}(e)$.

Denote by $[[v_b]]_{\Gamma_b}$ the jump of v_b on $e \in \Gamma_h$; i.e.,

$$[[v_b]]_{\Gamma_h} = v_b|_{\partial T_L \cap \Gamma_h} - v_b|_{\partial T_R \cap \Gamma_h}.$$

For any $v, w \in V_h$, let us introduce the following bilinear forms:

$$\begin{split} s(v,w) &= \rho \sum_{T \in \mathcal{T}_h} h_T^{-1} \langle Q_b v_0 - v_b, Q_b w_0 - w_b \rangle_{\partial T}, \\ a(v,w) &= \sum_{T \in \mathcal{T}_h} (a \nabla_w v, \nabla_w w)_T + s(v,w), \end{split}$$

where $\rho > 0$ is the stabilization parameter.

Weak Galerkin Algorithm 1. A weak Galerkin numerical scheme for the weak formulation (1.5) of the model problem (1.1)–(1.4) can be obtained by seeking $u_h = \{u_0, u_b\} \in V_h$ such that $u_b = Q_b g$ on $\partial \Omega \setminus \Gamma_h$, $[[u_b]]_{\Gamma_h} = Q_b g_D$ satisfying

$$a(u_h, v) = (f, v_0) + \sum_{e \in \Gamma_h \cap \Omega_1} \langle g_N, v_b \rangle_e + \sum_{e \in \Gamma_h \cap \Omega_2} \langle g_N, v_b \rangle_e, \quad \forall v \in V_h^0.$$

$$(3.5)$$

For any $v \in V_h$, the weak Galerkin scheme (3.5) induces a seminorm given by

$$\|v\|^2 = a(v, v).$$
 (3.6)

Lemma 3.1. For any $v \in V_h^0$, the seminorm defined in (3.6) is a norm, provided that the meshsize h is sufficiently small.

Proof. The proof is similar to the proof of Lemma 5.1 in [41]. \Box

Theorem 3.2. The weak Galerkin scheme (3.5) has one and only one numerical solution.

Proof. It suffices to prove the uniqueness. Assume that $u_h^{(1)}$ and $u_h^{(2)}$ are two different solutions of (3.5), then the function $\varepsilon_h = u_h^{(1)} - u_h^{(2)}$ satisfies the following equation:

$$a(\varepsilon_h, v) = 0, \quad \forall v \in V_h^0.$$
 (3.7)

By letting $v = \varepsilon_h \in V_h^0$ in (3.7) yields

$$a(\varepsilon_h, \varepsilon_h) = 0$$
,

which, together with (3.6) and Lemma 3.1, gives rise to $\varepsilon_h = 0$ and further $u_h^{(1)} = u_h^{(2)}$. This completes the proof of the theorem.

4. Error equation

This section aims to derive an error equation for the weak Galerkin scheme (3.5). For simplicity of analysis, we assume that the coefficient tensor a in the model problem (1.1)–(1.4) is piecewise constant with respect to the finite element partition \mathcal{T}_h . The following analysis can be generalized to piecewise smooth tensor a without technical difficulty.

Let u and $u_h \in V_h$ be the exact solution of the model problem (1.1)–(1.4) and the numerical solution of the WG scheme (3.5), respectively. On each element $T \in \mathcal{T}_h$, denote by Q_0 the usual L^2 projection operator onto $P_k(T)$. Recall that $Q_b u$ takes different values as seen from the left side and right side of the edge $e \in \Gamma_h$ and takes a single value on the edge $e \in \mathcal{E}_h \setminus \Gamma_h$. We further define a projection $Q_h u$ onto V_h such that

$$Q_h u = \{Q_0 u, Q_h u\}.$$

Denote by \mathbb{Q}_h the L^2 projection operator onto $[P_{k-1}(T)]^2$.

Let e_h be the error function defined by

$$e_h = Q_h u - u_h = \{e_0, e_h\} = \{Q_0 u - u_0, Q_h u - u_h\}.$$

Lemma 4.1 ([41]). For any $\psi \in [P_{k-1}(T)]^2$, there holds

$$(\nabla_w Q_h u, \pmb{\psi})_T = (\nabla u, \pmb{\psi})_T + \langle Q_b u - u, \pmb{\psi} \cdot \mathbf{n} \rangle_{\partial T}.$$

Note that $\langle Q_b u - u, \psi \cdot \mathbf{n} \rangle_{\partial T} \neq 0$ when the boundary ∂T consists of at least one curved edge.

Lemma 4.2. For any $v \in V_h^0$, the error function e_h satisfies the following equation

$$a(e_h, v) = s(Q_h u, v) + \ell_1(u, v) + \ell_2(u, v),$$

where $\ell_1(u,v)$ and $\ell_2(u,v)$ are given by

$$\begin{split} & \mathcal{\ell}_1(u,v) \, = \, \sum_{T \in \mathcal{T}_h} \langle (a \nabla u - a \mathbb{Q}_h \nabla u) \cdot \mathbf{n}, v_0 - v_b \rangle_{\partial T}, \\ & \mathcal{\ell}_2(u,v) \, = \, \sum_{T \in \mathcal{T}_h} \langle Q_b u - u, a \nabla_w v \cdot \mathbf{n} \rangle_{\partial T}. \end{split}$$

Note that the last term $\ell_2(u, v) = 0$ when the boundary ∂T is straight edge.

Proof. By testing the model Eq. (1.1) against v_0 and then using the usual integration by parts, there holds

$$\begin{split} &\sum_{T \in \mathcal{T}_h} (-\nabla \cdot (a \nabla u), v_0)_T \\ &= \sum_{T \in \mathcal{T}_h} (a \nabla u, \nabla v_0)_T - \langle a \nabla u \cdot \mathbf{n}, v_0 \rangle_{\partial T} \\ &= \sum_{T \in \mathcal{T}_h} (a \nabla u, \nabla v_0)_T - \langle a \nabla u \cdot \mathbf{n}, v_0 - v_b \rangle_{\partial T} - \sum_{e \in \Gamma_h} \langle a \nabla u \cdot \mathbf{n}, v_b \rangle_e \\ &= \sum_{T \in \mathcal{T}_h} (a \nabla u, \nabla v_0)_T - \langle a \nabla u \cdot \mathbf{n}, v_0 - v_b \rangle_{\partial T} - \sum_{e \in \Gamma_h \cap \Omega_1} \langle [[a \nabla u \cdot \mathbf{n}]], v_b \rangle_e \\ &- \sum_{e \in \Gamma_h \cap \Omega_2} \langle [[a \nabla u \cdot \mathbf{n}]], v_b \rangle_e \\ &= \sum_{T \in \mathcal{T}_h} (a \nabla u, \nabla v_0)_T - \langle a \nabla u \cdot \mathbf{n}, v_0 - v_b \rangle_{\partial T} - \sum_{e \in \Gamma_h \cap \Omega_1} \langle g_N, v_b \rangle_e \\ &- \sum_{e \in \Gamma_h \cap \Omega_2} \langle g_N, v_b \rangle_e, \end{split}$$

$$(4.1)$$

where we also used the boundary condition (1.4) and the fact that v_b is single valued on $e \in \mathcal{E}_h \setminus \Gamma_h$.

For the first term on the last line of (4.1), using the definition of \mathbb{Q}_h , the usual integration by parts and (2.2) yields

$$(a\nabla u, \nabla v_0)_T = (a\mathbb{Q}_h \nabla u, \nabla v_0)_T$$

$$= -(\nabla \cdot (a\mathbb{Q}_h \nabla u), v_0)_T + \langle a\mathbb{Q}_h \nabla u \cdot \mathbf{n}, v_0 \rangle_{\partial T}$$

$$= (a\mathbb{Q}_h \nabla u, \nabla_w v)_T - \langle v_b, a\mathbb{Q}_h \nabla u \cdot \mathbf{n} \rangle_{\partial T} + \langle a\mathbb{Q}_h \nabla u \cdot \mathbf{n}, v_0 \rangle_{\partial T}$$

$$= (a\mathbb{Q}_h \nabla u, \nabla_w v)_T + \langle a\mathbb{Q}_h \nabla u \cdot \mathbf{n}, v_0 - v_b \rangle_{\partial T}.$$

$$(4.2)$$

Substituting (4.2) into (4.1) and then using the definition of \mathbb{Q}_h , Lemma 4.1 with $\psi = a\nabla_w v$ give

$$\begin{split} &\sum_{T \in \mathcal{T}_{h}} (-\nabla \cdot (a\nabla u), v_{0})_{T} \\ &= \sum_{T \in \mathcal{T}_{h}} (a\mathbb{Q}_{h} \nabla u, \nabla_{w} v)_{T} - \langle v_{0} - v_{b}, a(\nabla u - \mathbb{Q}_{h} \nabla u) \cdot \mathbf{n} \rangle_{\partial T} \\ &- \sum_{e \in \Gamma_{h} \cap \Omega_{1}} \langle g_{N}, v_{b} \rangle_{e} - \sum_{e \in \Gamma_{h} \cap \Omega_{2}} \langle g_{N}, v_{b} \rangle_{e} \\ &= \sum_{T \in \mathcal{T}_{h}} (a\nabla u, \nabla_{w} v)_{T} - \ell_{1}(u, v) - \sum_{e \in \Gamma_{h} \cap \Omega_{1}} \langle g_{N}, v_{b} \rangle_{e} - \sum_{e \in \Gamma_{h} \cap \Omega_{2}} \langle g_{N}, v_{b} \rangle_{e} \\ &= \sum_{T \in \mathcal{T}_{h}} (\nabla_{w} \mathcal{Q}_{h} u, a\nabla_{w} v)_{T} - \langle \mathcal{Q}_{b} u - u, a\nabla_{w} v \cdot \mathbf{n} \rangle_{\partial T} - \ell_{1}(u, v) \\ &- \sum_{e \in \Gamma_{h} \cap \Omega_{1}} \langle g_{N}, v_{b} \rangle_{e} - \sum_{e \in \Gamma_{h} \cap \Omega_{2}} \langle g_{N}, v_{b} \rangle_{e} \\ &= \sum_{T \in \mathcal{T}_{h}} (\nabla_{w} \mathcal{Q}_{h} u, a\nabla_{w} v)_{T} - \ell_{2}(u, v) - \ell_{1}(u, v) - \sum_{e \in \Gamma_{h} \cap \Omega_{1}} \langle g_{N}, v_{b} \rangle_{e} \\ &- \sum_{e \in \Gamma_{h} \cap \Omega_{2}} \langle g_{N}, v_{b} \rangle_{e}. \end{split}$$

$$(4.3)$$

Using (1.1), (3.5) and $e_h = Q_h u - u_h$, one arrives at

$$a(e_h, v) = s(Q_h u, v) + \ell_1(u, v) + \ell_2(u, v),$$

which completes the proof of the lemma. \Box

5. Technical results

This section is devoted to presenting some technical results. To this end, let \mathcal{T}_h be a curved shape regular partition satisfying the shape regularity assumptions A1–A4. For any $T \in \mathcal{T}_h$ and $\phi \in H^1(T)$, the following trace inequality holds true [41]:

$$\|\phi\|_{a}^{2} \lesssim h_{T}^{-1} \|\phi\|_{T}^{2} + h_{T} \|\nabla\phi\|_{T}^{2}. \tag{5.1}$$

If ϕ is a polynomial on any $T \in \mathcal{T}_h$, using the inverse inequality, there holds [41]

$$\|\phi\|_{e}^{2} \lesssim h_{T}^{-1} \|\phi\|_{T}^{2}. \tag{5.2}$$

Lemma 5.1. Let \mathcal{T}_h be a curved finite element partition of Ω that is shape regular as described in [41]. For any $\phi \in H^{k+1}(\Omega)$, there holds [41]

$$\sum_{T \in \mathcal{T}_{c}} h_{T}^{2s} \|Q_{0}\phi - \phi\|_{s,T}^{2} \lesssim h^{2k+2} \|\phi\|_{k+1}^{2}, \quad 0 \le s \le 2,$$
(5.3)

$$\sum_{T \in \mathcal{T}_{s}} h_{T}^{2s} \|\nabla \phi - \mathbb{Q}_{h} \nabla \phi\|_{s,T}^{2} \lesssim h^{2k} \|\phi\|_{k+1}^{2}, \quad 0 \leq s \leq 2,$$
(5.4)

$$\sum_{T \in T_{-}} \|Q_{b}\phi - \phi\|_{\partial T}^{2} \lesssim h^{2k-1} \|\phi\|_{k}^{2}. \tag{5.5}$$

Lemma 5.2. For any $v \in V_h$, $\phi \in H^1(T)$ and $\mathbf{q} \in [P_{k-1}(T)]^2$, there holds [41]

$$h_T^{-1} \|v_0 - v_b\|_{\partial T}^2 \lesssim \|\nabla v_0\|_T^2 + h_T^{-1} \|Q_b v_0 - v_b\|_{\partial T}^2, \tag{5.6}$$

$$\|\nabla v_0\|_T^2 \lesssim \|\nabla_w v\|_T^2 + h_T^{-1} \|Q_b v_0 - v_b\|_{\partial T}^2, \tag{5.7}$$

$$|\langle \phi - Q_b \phi, \mathbf{q} \cdot \mathbf{n} \rangle_e| \lesssim \begin{cases} h_e^{1/2} ||\phi - Q_b \phi||_{\partial T} ||\mathbf{q}||_T, & \text{for } k \ge 1, \\ h_e^{3/2} ||\phi - Q_b \phi||_{\partial T} (||\mathbf{q}||_T + ||\nabla \mathbf{q}||_T), & \text{for } k \ge 2. \end{cases}$$

$$(5.8)$$

Lemma 5.3. For any $u \in H^{k+1}(\Omega_i)$ for i = 1, 2 and $v \in V_h$, there holds

$$|s(Q_h u, v)| \lesssim h^k (||u||_{k+1, \Omega_1} + ||u||_{k+1, \Omega_2}) ||v||_{l}, \tag{5.9}$$

$$|\ell_1(u,v)| \lesssim h^k(||u||_{k+1,\Omega_1} + ||u||_{k+1,\Omega_2})||v||, \tag{5.10}$$

$$\left|\ell_{2}(u,v)\right| \lesssim h^{k}(\|u\|_{k+1,\Omega_{1}} + \|u\|_{k+1,\Omega_{2}})\|\|v\|, \tag{5.11}$$

where $\ell_1(u,v)$ and $\ell_2(u,v)$ are given by Lemma 4.2.

Proof. To derive the first inequality (5.9), it follows from the Cauchy–Schwarz inequality, the property of Q_h , (5.1) and (5.3) that

$$\begin{split} |s(Q_h u, v)| &= |\rho \sum_{T \in \mathcal{T}_h} h_T^{-1} \langle Q_b(Q_0 u) - Q_b u, Q_b v_0 - v_b \rangle_{\partial T}| \\ &\lesssim \left(\rho \sum_{T \in \mathcal{T}_h} h_T^{-1} \|Q_b(Q_0 u - u)\|_{\partial T}^2\right)^{\frac{1}{2}} \left(\rho \sum_{T \in \mathcal{T}_h} h_T^{-1} \|Q_b v_0 - v_b\|_{\partial T}^2\right)^{\frac{1}{2}} \\ &\lesssim \left(\sum_{T \in \mathcal{T}_h} h_T^{-1} \|Q_0 u - u\|_{\partial T}^2\right)^{\frac{1}{2}} \|\|v\|\| \\ &\lesssim \left(\sum_{T \in \mathcal{T}_h} h_T^{-2} \|Q_0 u - u\|_T^2 + |Q_0 u - u|_{1,T}^2\right)^{\frac{1}{2}} \|\|v\|\| \\ &\lesssim h^k(\|u\|_{k+1,\Omega_1} + \|u\|_{k+1,\Omega_2}) \|\|v\|\|. \end{split}$$

To analyze the second inequality (5.10), using the Cauchy-Schwarz inequality (5.1), (5.4), (5.5), (5.7) and (3.6), there holds

$$\begin{split} &|\mathcal{E}_{1}(u,v)| \\ &= |\sum_{T \in \mathcal{T}_{h}} \langle a \nabla u \cdot \mathbf{n} - a \mathbb{Q}_{h} \nabla u \cdot \mathbf{n}, v_{0} - v_{b} \rangle_{\partial T}| \\ &\lesssim \left(\sum_{T \in \mathcal{T}_{h}} h_{T} \| a \nabla u - a \mathbb{Q}_{h} \nabla u \|_{\partial T}^{2}\right)^{\frac{1}{2}} \left(\sum_{T \in \mathcal{T}_{h}} h_{T}^{-1} \| v_{0} - v_{b} \|_{\partial T}^{2}\right)^{\frac{1}{2}} \\ &\lesssim \left(\sum_{T \in \mathcal{T}_{h}} \| a \nabla u - a \mathbb{Q}_{h} \nabla u \|_{T}^{2} + h_{T}^{2} \| a \nabla u - a \mathbb{Q}_{h} \nabla u \|_{1,T}^{2}\right)^{\frac{1}{2}} \\ &\cdot \left(\sum_{T \in \mathcal{T}_{h}} h_{T}^{-1} \| Q_{b} v_{0} - v_{b} \|_{\partial T}^{2} + h_{T}^{-1} \| v_{0} - Q_{b} v_{0} \|_{\partial T}^{2}\right)^{\frac{1}{2}} \\ &\lesssim h^{k} (\| u \|_{k+1,\Omega_{1}} + \| u \|_{k+1,\Omega_{2}}) \left(\| v \|^{2} + \sum_{T \in \mathcal{T}_{h}} \| \nabla v_{0} \|_{T}^{2}\right)^{\frac{1}{2}} \\ &\lesssim h^{k} (\| u \|_{k+1,\Omega_{1}} + \| u \|_{k+1,\Omega_{2}}) \left(\| v \|^{2} + \sum_{T \in \mathcal{T}_{h}} \| \nabla_{w} v \|_{T}^{2} + h_{T}^{-1} \| Q_{b} v_{0} - v_{b} \|_{\partial T}^{2}\right)^{\frac{1}{2}} \\ &\lesssim h^{k} (\| u \|_{k+1,\Omega_{1}} + \| u \|_{k+1,\Omega_{2}}) \left(\| v \|^{2} + \| v \|^{2} + \| v \|^{2}\right)^{\frac{1}{2}} \\ &\lesssim h^{k} (\| u \|_{k+1,\Omega_{1}} + \| u \|_{k+1,\Omega_{2}}) \| v \|. \end{split}$$

To estimate the last estimate (5.11), from (5.8), the Cauchy-Schwarz inequality, (5.5) and (3.6), there yields

$$\begin{split} |\ell_2(u,v)| &= |\sum_{T \in \mathcal{T}_h} \langle Q_b u - u, a \nabla_w v \cdot \mathbf{n} \rangle_{\partial T}| \\ &\lesssim \sum_{T \in \mathcal{T}_h} h_T^{\frac{1}{2}} \|Q_b u - u\|_{\partial T} \|a \nabla_w v\|_T \\ &\lesssim h^{\frac{1}{2}} \Big(\sum_{T \in \mathcal{T}_h} \|Q_b u - u\|_{\partial T}^2\Big)^{\frac{1}{2}} \Big(\sum_{T \in \mathcal{T}_h} \|a \nabla_w v\|_T^2\Big)^{\frac{1}{2}} \\ &\lesssim h^k (\|u\|_{k+1,\Omega_1} + \|u\|_{k+1,\Omega_2}) \|v\|. \end{split}$$

This completes the proof of the lemma. \Box

6. Error estimates

The objective of this section is to establish some optimal order error estimates for the numerical approximation.

Theorem 6.1. Let u and $u_h \in V_h$ be the exact solution of the model problem (1.1)–(1.4) and the numerical solution of the WG scheme (3.5), respectively. Assume that the exact solution u satisfies $u \in H^{k+1}(\Omega_i)$ for i = 1, 2. Then, the following error estimate holds true

$$\|e_h\| \lesssim h^k(\|u\|_{k+1,\Omega_1} + \|u\|_{k+1,\Omega_2}).$$
 (6.1)

Proof. By taking $v = e_h$ in Lemma 4.2, one arrives at

$$a(e_h, e_h) = s(Q_h u, e_h) + \ell_1(u, e_h) + \ell_2(u, e_h).$$

It follows from (3.6) and Lemma 5.3 with $v = e_h$ that

$$|||e_h|||^2 \lesssim h^k(||u||_{k+1,Q_1} + ||u||_{k+1,Q_2})|||e_h||_{k+1,Q_2}$$

This completes the proof. \Box

Corollary 6.2. Under the assumptions of Theorem 6.1, the following error estimate holds true

$$\|\nabla e_0\| \lesssim h^k(\|u\|_{k+1,\Omega_1} + \|u\|_{k+1,\Omega_2}). \tag{6.2}$$

Proof. It follows from (5.7) and (3.6) that

$$\begin{split} \|\nabla e_0\| & \lesssim \left(\sum_{T \in \mathcal{T}_h} \|\nabla_w e_h\|_T^2 + h_T^{-1} \|Q_b e_0 - e_b\|_{\partial T}^2\right)^{\frac{1}{2}} \\ & \lesssim \|\|e_h\|\|, \end{split}$$

which, together with Theorem 6.1, gives rise to (6.2). This completes the proof of the corollary. \Box

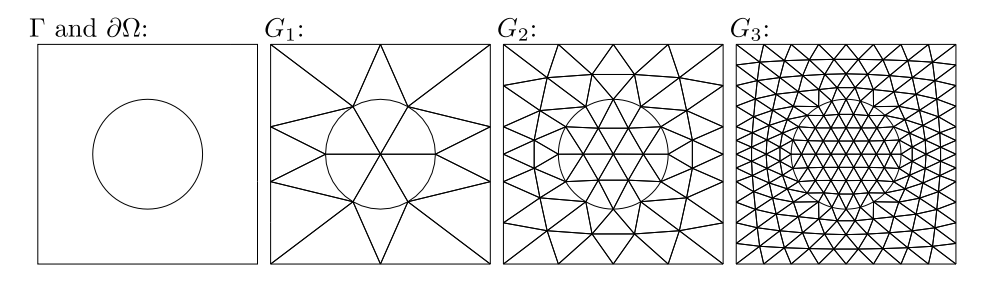


Fig. 7.1. The interface Γ and the first three grids for the computation in Tables 7.1–7.5.

Theorem 6.3. Let $u \in H^{k+1}(\Omega_i)$ for i = 1, 2 be the exact solution of (1.1)–(1.4) and $u_h \in V_h$ be the numerical solution of WG scheme (3.5), respectively. Assume that the dual problem of (1.1)–(1.4) with $\Gamma = \emptyset$ satisfies the H^2 regular property as described in [28]. Then, the following error estimate holds true

$$||e_0|| \lesssim h^{k+1}(||u||_{k+1,\Omega_1} + ||u||_{k+1,\Omega_2}). \tag{6.3}$$

Proof. The proof is similar to the proof of Theorem 6.4 in [42]. \square

To establish the error estimate for e_h , we define the following semi-norm

$$\|e_b\|_{\mathcal{E}_h} = \left(\sum_{T \in \mathcal{T}_h} h_T \|e_b\|_{\partial T}^2\right)^{1/2}.$$
 (6.4)

Theorem 6.4. In the assumptions of Theorem 6.3, we have the following error estimate

$$\|e_b\|_{\mathcal{E}_h} \lesssim h^{k+1}(\|u\|_{k+1,\Omega_1} + \|u\|_{k+1,\Omega_2}).$$
 (6.5)

Proof. Using the triangle inequality, the trace inequality (5.2), Theorem 6.1 and Theorem 6.3, there holds

$$\begin{split} \|e_b\|_{\mathcal{E}_h} &= \left(\sum_{T \in \mathcal{T}_h} h_T \|e_b\|_{\partial T}^2\right)^{\frac{1}{2}} \\ &\lesssim \left(\sum_{T \in \mathcal{T}_h} h_T \|Q_b e_0\|_{\partial T}^2 + h_T \|e_b - Q_b e_0\|_{\partial T}^2\right)^{\frac{1}{2}} \\ &\lesssim \left(\sum_{T \in \mathcal{T}_h} \|e_0\|_T^2\right)^{\frac{1}{2}} + \left(\sum_{T \in \mathcal{T}_h} \rho_1 h_T \|e_b - Q_b e_0\|_{\partial T}^2\right)^{\frac{1}{2}} \\ &\lesssim \|e_0\| + h \|e_h\| \\ &\lesssim h^{k+1} (\|u\|_{k+1,\Omega_1} + \|u\|_{k+1,\Omega_2}). \end{split}$$

This completes the proof of the theorem. \Box

7. Numerical experiments

This section presents some numerical experiments to validate the accuracy of the developed convergence theory. In the first numerical test, we solve the elliptic interface problem (1.5) in a global weak formulation: Find $u \in H^1(\Omega)$ with

$$\Omega = (-2, 2) \times (-2, 2),$$

such that $u|_{\partial Q} = 2 - (x^2 + y^2)^3$ and

$$(a\nabla u, \nabla v) = (36(x^2 + y^2)^2, v), \quad \forall v \in H_0^1(\Omega),$$
 (7.1)

where

$$a(x,y) = \begin{cases} \mu, & \text{if } x^2 + y^2 \le 1, \\ 1, & \text{if } x^2 + y^2 > 1. \end{cases}$$
 (7.2)

(7.2) implicitly defines $\Gamma = \{(x, y) : x^2 + y^2 = 1\}.$

The weak solution of (7.1) is

$$u(x,y) = \begin{cases} \mu^{-1}(1+\mu-(x^2+y^2)^3) & \text{if } x^2+y^2 < 1, \\ 1 & \text{if } x^2+y^2 = 1, \\ 2-(x^2+y^2)^3 & \text{if } x^2+y^2 > 1. \end{cases}$$
(7.3)

Table 7.1 The error of P_1 elements for (7.1) on triangular grids (Fig. 7.1).

G_i	$\ Q_0u - u_0\ _{0,a}$	Rate	$\ \nabla_w(Q_hu-u_h)\ _{0,a^2}$	Rate
	By the P_1 - P_2 - P_2^2 finite ele	ment, $\mu = 10^{-4}$ in (7.2).		
4	0.1024E-01	4.0	0.1348E+00	2.9
5	0.6225E-03	4.0	0.1662E-01	3.0
6	0.3837E-04	4.0	0.2062E-02	3.0
	By the P_1 - P_2 - P_2^2 finite element, $\mu = 1$ in (7.2).			
4	0.4209E-02	4.0	0.1348E+00	2.9
5	0.2675E-03	4.0	0.1733E-01	3.0
6	0.1688E-04	4.0	0.2200E-02	3.0
	By the P_1 - P_2 - P_2^2 finite element, $\mu = 10^4$ in (7.2).			
4	0.1503E+00	4.0	0.1348E+00	2.9
5	0.9339E-02	4.0	0.1733E-01	3.0
6	0.5956E-03	4.0	0.2200E-02	3.0

Table 7.2 The error of P_2 elements for (7.3) on triangular grids (Fig. 7.1).

G_i	$ Q_0u - u_0 _{0,a}$	Rate	$\ \nabla_w(Q_hu-u_h)\ _{0,a^2}$	Rate	
	By the P_2 - P_3 - P_3^2 finite ele	ement, $\mu = 10^{-4}$ in (7.2).			
3	0.3400E-02	5.0	0.2364E-01	4.0	
4	0.1032E-03	5.0	0.1406E-02	4.1	
5	0.3095E-05	5.1	0.8373E-04	4.1	
	By the P_2 - P_3 - P_3^2 finite element, $\mu = 1$ in (7.2).				
3	0.1092E-02	4.9	0.2361E-01	4.0	
4	0.3545E-04	4.9	0.1488E-02	4.0	
5	0.1141E-05	5.0	0.9387E-04	4.0	
	By the P_2 - P_3 - P_3^2 finite element, $\mu = 10^4$ in (7.2).				
2	0.5463E-01	5.2	0.3779E+00	4.1	
3	0.1317E-02	5.4	0.2363E-01	4.0	
4	0.3647E-04	5.2	0.1488E-02	4.0	

We note that with the careful construction (7.3), the weak solution of (7.1) is the strong solution of (1.1)–(1.4) as

$$u|_{\Gamma} \neq 0$$
, $\mu \partial_{\mathbf{n}}^{(n)} u|_{\Gamma^{-}} = \partial_{\mathbf{n}}^{(n)} u|_{\Gamma^{-}}$, $n = 1, 2, ...$,

where the interface $\Gamma = \{(x, y) : x^2 + y^2 = 1\}$, **n** is the unit outward normal vector on Γ , and $\partial_{\mathbf{n}}^{(n)} u$ is the *n*th directional derivative of u in the direction **n**.

Since the significant digits of the computer double precision format are limited, we could not reach enough levels of order five or above convergence for the P_k - P_{k-1} - P_{k-1}^2 weak Galerkin finite elements. Instead, we use a two-order superconvergent P_k - P_{k+1} - P_{k+1}^2 weak Galerkin method, i.e., $v_b|_e \in V_b(e,k+1)$ in (3.3) and $\nabla_w v = \nabla_{w,k+1,T}$ in (3.4). This way, using lower-degree polynomials, we can compute order-eight convergent solutions for the curved-edge interface problem (7.1).

In Table 7.1, we list the results of the P_1 - P_2 - P_2^2 finite element for solving the interface problem (7.1) on meshes shown in Fig. 7.1. Here, to cancel somewhat the difference of solutions with different μ , we use a weighted norm to measure the error,

$$||u||_{0,a}^2 = \int_O a(x, y)u^2(x, y)dx dy.$$

Supposedly the P_1 finite element converges at order 2 in L^2 norm and order 1 in H^1 norm, respectively. But as the method of two-order superconvergence, the P_1 finite element solution converges two orders above the optimal order, in both norms, in Table 7.1.

In Table 7.2, we list the results of the P_2 - P_3 - P_3^2 finite element for solving the interface problem (7.1) on meshes shown in Fig. 7.1. The optimal order of convergence of the P_2 finite element is order 3 and order 2 in L^2 norm and H^1 norm, respectively. Here in Table 7.2, the finite element solution converges two orders above the optimal order. It seems from Table 7.2 that the error bound is independent of the size of jump of the coefficient a in the interface problem (7.1).

In Fig. 7.2, we plot the P_2 solution for the interface problem (7.1), where $\mu = 10^{-3}$, on the third grid G_3 in Fig. 7.1. We can see that the normal derivative of the solution jumps to one thousand times large at the interface circle, i.e., a sharp turn there. Also in Fig. 7.2, we plot the error of above solution on the same mesh. The error indicates that the method matches the interface curve well and the error bound is truly independent of the μ -jump.

In Table 7.3, we list the results of the P_3 - P_4 - P_4 finite element for solving the interface problem (7.1) on meshes shown in Fig. 7.1. Again in Table 7.4, the finite element solution converges at two orders above the optimal order, in both norms.

In Table 7.4, we list the results of the P_4 - P_5 - P_5^2 finite element for solving the interface problem (7.1) on meshes shown in Fig. 7.1. Again in Table 7.4, the finite element solution converges at two orders above the optimal order.

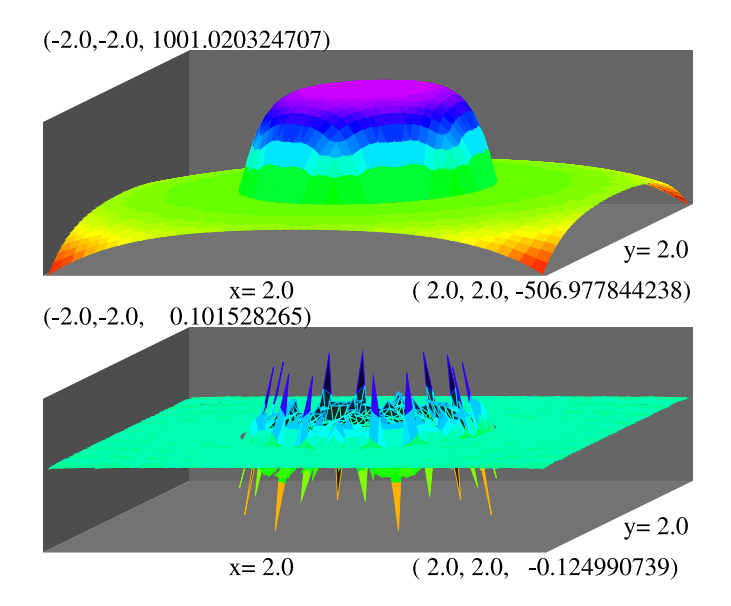


Fig. 7.2. Top: The P_2 finite element solution for (7.1) with $\mu = 10^{-3}$ in (7.2) on the third grid G_3 in Fig. 7.1. Bottom: The error of the solution above.

Table 7.3 The error of P_3 elements for (7.1) on triangular grids (Fig. 7.1).

G_{i}	$\ Q_0u - u_0\ _{0,a}$	Rate	$\ \nabla_w(Q_h u - u_h)\ _{0,a^2}$	Rate	
	By the P_3 - P_4 - P_4^2 finite ele	ement, $\mu = 10^{-4}$ in (7.2).			
3	0.5685E-04	6.1	0.3073E-03	5.0	
4	0.8292E-06	6.1	0.9668E-05	5.0	
5	0.1210E-07	6.1	0.3021E-06	5.0	
	By the P_3 - P_4 - P_4^2 finite element, $\mu = 1$ in (7.2).				
3	0.8999E-05	6.0	0.3068E-03	5.0	
4	0.1441E-06	6.0	0.9655E-05	5.0	
5	0.2360E-08	5.9	0.3052E-06	5.0	
	By the P_3 - P_4 - P_4^2 finite element, $\mu = 10^2$ in (7.2).				
2	0.5741E-03	6.2	0.1006E-01	5.2	
3	0.8996E-05	6.0	0.3072E-03	5.0	
4	0.1441E-06	6.0	0.9665E-05	5.0	

Table 7.4 The error of P_4 elements for (7.1) on triangular grids (Fig. 7.1).

G_i	$\ Q_0u - u_0\ _{0,a}$	Rate	$\ \nabla_w(Q_hu-u_h)\ _{0,a^2}$	Rate	
	By the P_4 - P_5 - P_5^2 finite ele	ement, $\mu = 10^{-4}$ in (7.2).			
2	0.1010E-03	7.3	0.8618E-04	6.5	
3	0.6374E-06	7.3	0.1009E-05	6.4	
4	0.4795E-08	7.1	0.1258E-07	6.4	
	By the P_3 - P_4 - P_4^2 finite element, $\mu = 1$ in (7.2).				
1	0.3672E-03	0.0	0.7482E-02	0.0	
2	0.2404E-05	7.3	0.8498E-04	6.5	
3	0.1695E-07	7.1	0.1042E-05	6.3	
	By the P_3 - P_4 - P_4^2 finite element, $\mu = 10$ in (7.2).				
1	0.3406E-03	0.0	0.7541E-02	0.0	
2	0.2254E-05	7.2	0.8560E-04	6.5	
3	0.1612E-07	7.1	0.1049E-05	6.4	

Finally, in Table 7.5, we list the results of the P_5 - P_6 - P_6^2 finite element for solving the interface problem (7.1) on meshes shown in Fig. 7.1. The finite element solution converges at order eight, two orders above the optimal order, in L^2 norm, when $\mu = 10^{-1}$. But when the error reaches 10^{-9} size, the computer accuracy is exhausted that we have a slightly less order of convergence at the last level, when $\mu = 1$ (smooth solution) and $\mu = 2$ (a derivative jump solution.)

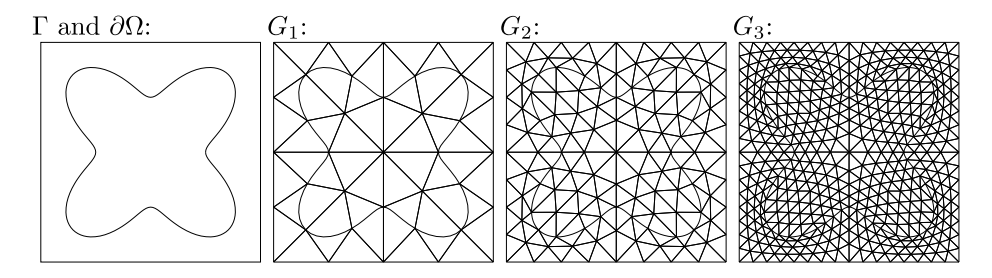


Fig. 7.3. The interface Γ and the first three grids for the computation in Tables 7.6–7.9.

Table 7.5 The error of P_5 elements for (7.1) on triangular grids (Fig. 7.1).

G_i	$ Q_0u - u_0 _{0,a}$	Rate	$\ \nabla_w(Q_hu-u_h)\ _{0,a^2}$	Rate
	By the P_5 - P_6 - P_6^2 finite ele	ement, $\mu = 10^{-4}$ in (7.2).		
1	0.9320E-03	0.0	0.5672E-03	0.0
2	0.2808E-05	8.4	0.3440E-05	7.4
3	0.1028E-07	8.1	0.3200E-07	6.7
	By the P_5 - P_6 - P_6^2 finite electrons	ement, $\mu = 1$ in (7.2).		
1	0.2238E-04	0.0	0.5576E-03	0.0
2	0.8150E-07	8.1	0.3325E-05	7.4
3	0.4517E-09	7.5	0.2190E-07	7.2
	By the $P_5 - P_6 - P_6^2$ finite element, $\mu = 2$ in (7.2).			
1	0.2159E-04	0.0	0.5585E-03	0.0
2	0.7879E-07	8.1	0.3335E-05	7.4
3	0.4194E-09	7.6	0.2230E-07	7.2

Table 7.6 The error of P_1 elements for (7.6) on grids shown in Fig. 7.3.

G_i	$\ Q_0u - u_0\ _{0,a}$	Rate	$\ \nabla_w(Q_hu-u_h)\ _{0,a^2}$	Rate	
	By the P_1 - P_2 - P_2^2 finite ele	ement, $\mu = 10^{-2}$ in (7.5).			
4	0.5271E-02	4.0	0.1129E+00	3.0	
5	0.3371E-03	4.0	0.1386E-01	3.0	
6	0.2174E-04	4.0	0.1716E-02	3.0	
	By the P_1 - P_2 - P_2^2 finite element, $\mu = 1$ in (7.5).				
4	0.4209E-02	4.0	0.1348E+00	2.9	
5	0.2675E-03	4.0	0.1733E-01	3.0	
6	0.1688E-04	4.0	0.2200E-02	3.0	
	By the P_1 - P_2 - P_2^2 finite element, $\mu = 10^2$ in (7.5).				
4	0.4062E-02	3.9	0.1162E+00	3.1	
5	0.2727E-03	3.9	0.1408E-01	3.0	
6	0.1816E-04	3.9	0.1731E-02	3.0	

In the second numerical test, we solve the interface problem (1.5) with a lightly irregular interface curve: Find $u \in H^1(\Omega)$ such that $u|_{\partial\Omega} = r^4(r-3+\cos(4\theta))$ and

$$(a\nabla u, \nabla v) = (48r^2 - 25r^3, v) \quad \forall v \in H_0^1(\Omega),$$
 (7.4)

where $r = \sqrt{x^2 + y^2}$, $\tan \theta = y/x$ and

$$a(x,y) = \begin{cases} \mu & \text{if } r < 3 - \cos(4\theta), \\ 1 & \text{if } r \ge 3 - \cos(4\theta), \end{cases}$$

$$\Omega = (-4,4) \times (-4,4). \tag{7.5}$$

The weak solution of (7.4) is

$$u(x,y) = \begin{cases} \mu^{-1} r^4 (r - 3 + \cos(4\theta)) & \text{if } r < 3 - \cos(4\theta), \\ r^4 (r - 3 + \cos(4\theta)) & \text{if } r \ge 3 - \cos(4\theta). \end{cases}$$
 (7.6)

The interface is $\Gamma = \{(x, y) : r = 3 - \cos(4\theta)\}$, shown in Fig. 7.3.

Table 7.7 The error of P_2 elements for (7.6) on grids shown in Fig. 7.3.

G_i	$\ Q_0u - u_0\ _{0,a}$	Rate	$\ \nabla_w(Q_hu-u_h)\ _{0,a^2}$	Rate
	By the P_2 - P_3 - P_3^2 finite ele	ement, $\mu = 10^{-2}$ in (7.5).		
3	0.6259E-02	5.1	0.2519E-01	4.6
4	0.2035E-03	4.9	0.1214E-02	4.4
5	0.7258E-05	4.8	0.6503E-04	4.2
	By the P_2 - P_3 - P_3^2 finite ele	ement, $\mu = 1$ in (7.5).		
3	0.9359E-03	5.4	0.2179E-01	4.5
4	0.2705E-04	5.1	0.1101E-02	4.3
5	0.9088E-06	4.9	0.6097E-04	4.2
	By the P_2 - P_3 - P_3^2 finite element, $\mu = 10^2$ in (7.5).			
3	0.5124E-03	5.3	0.2464E-01	4.6
4	0.1606E-04	5.0	0.1203E-02	4.4
5	0.5719E-06	4.8	0.6470E-04	4.2

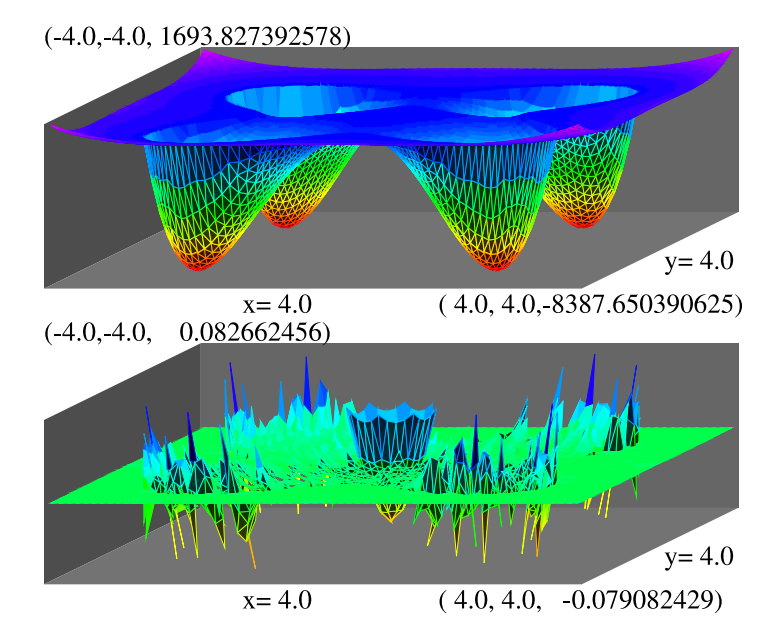


Fig. 7.4. Top: The P_2 finite element solution for (7.4) with $\mu = 10^{-2}$ in (7.5) on the second grid G_2 in Fig. 7.3. Bottom: The error of the solution above.

In Table 7.6, we list the computational errors of the P_1 - P_2 - P_2^2 finite element for solving the interface problem (7.4) on meshes shown in Fig. 7.3. The result is perfect, showing two-order superconvergence, jump-independent error bounds, and accurate interface approximation.

In Table 7.7, we list the errors of the P_2 - P_3 - P_3^2 finite element for solving the interface problem (7.4) on meshes shown in Fig. 7.3. The computation is accurate enough to show two-order superconvergence, jump-independent error bounds, and accurate interface approximation.

In Fig. 7.4, the P_2 solution for the second interface problem (7.4) is plotted. The solution jumps downward at the interface curve. We can see from the error graph of Fig. 7.4 that the error is independent of jump size of the coefficient μ . It is surprising that the error at the edge of the center hexagon (see the third graph in Fig. 7.3) is even larger than that at the interface. In fact, it shows our method approximates the interface very well so that the solution error is independent of the interface jump. On the other side, it shows our method is very accurate that the underline meshes must be smooth. Here, due to the geometry limitation, the meshes changed the pattern near the origin that even the regular hexagon and regular triangles are not the best mesh shapes there.

In Table 7.8, we list the errors of the P_3 - P_4 - P_4^2 finite element for solving the interface problem (7.4) on meshes shown in Fig. 7.3. The computation is barely accurate enough to show two-order superconvergence, jump-independent error bounds, and accurate interface approximation.

In Table 7.9, we list the errors of the P_4 - P_5 - P_5^2 finite element for solving the interface problem (7.4) on meshes shown in Fig. 7.3. The computation accuracy is reached that the third level L^2 errors do not reach the two orders above the optimal order, due to computer round-off. It is supposedly of order 7, if computed in a better accuracy computer.

Table 7.8 The error of P_3 elements for (7.6) on grids shown in Fig. 7.3.

G_i	$ Q_0u - u_0 _{0,a}$	Rate	$\ \nabla_w(Q_h u - u_h)\ _{0,a^2}$	Rate	
	By the P_3 - P_4 - P_4^2 finite ele	ement, $\mu = 10^{-2}$ in (7.5).			
1	0.7386E+00	0.0	0.1385E+01	0.0	
2	0.1382E-01	5.7	0.4572E-01	4.9	
3	0.1904E-03	6.2	0.1572E-02	4.9	
	By the $P_3 - P_4 - P_4^2$ finite element, $\mu = 1$ in (7.5).				
1	0.1078E+00	0.0	0.1190E+01	0.0	
2	0.2541E-02	5.4	0.4101E-01	4.9	
3	0.4467E-04	5.8	0.1349E-02	4.9	
	By the P_3 - P_4 - P_4^2 finite element, $\mu = 10^2$ in (7.5).				
1	0.5595E-01	0.0	0.1412E+01	0.0	
2	0.1201E-02	5.5	0.4627E-01	4.9	
3	0.2476E-04	5.6	0.1615E-02	4.8	

Table 7.9 The error of P_4 elements for (7.6) on grids shown in Fig. 7.3.

G_i	$\ Q_0 u - u_0\ _{0,a}$	Rate	$\ \nabla_w(Q_hu-u_h)\ _{0,a^2}$	Rate	
	By the P_4 - P_5 - P_5^2 finite ele	ement, $\mu = 2^{-1}$ in (7.5).			
1	0.2601E-01	0.0	0.2876E+00	0.0	
2	0.1893E-03	7.1	0.3930E-02	6.2	
3	0.4570E-05	5.4	0.3638E-04	6.8	
	By the P_4 - P_5 - P_5^2 finite element, $\mu = 1$ in (7.5).				
1	0.2173E-01	0.0	0.2818E+00	0.0	
2	0.1599E-03	7.1	0.3831E-02	6.2	
3	0.3966E-05	5.3	0.3579E-04	6.7	
	By the P_4 - P_5 - P_5^2 finite element, $\mu = 2$ in (7.5).				
1	0.1799E-01	0.0	0.2876E+00	0.0	
2	0.1344E-03	7.1	0.3941E-02	6.2	
3	0.3679E-05	5.2	0.3643E-04	6.8	

Data availability

Data will be made available on request.

References

- [1] B. Khoo, Z. Li, P. Lin, Interface Problems and Methods in Biological and Physical Flow, World Scientific, 2009.
- [2] T. Hou, Z. Li, S. Osher, H. Zhao, A hybrid method for moving interface problems with application to the Hele-Shaw flow, J. Comput. Phys. 134 (1997) 236–252.
- [3] A. Layton, Using integral equations and the immersed interface method to solve immersed boundary problems with stiff forces, Comput. Fluids 38 (2009) 266–272
- [4] J. Hesthaven, High-order accurate methods in time-domain computational electromagnetics: A review, Adv. Image Electron. Phys. 127 (2003) 59-123.
- [5] D. Chen, Z. Chen, C. Chen, W. Geng, G. Wei, MIBPB: a software package for electrostatic analysis, J. Comput. Chem. 32 (2011) 756-770.
- [6] Z. Li, The immersed interface method using a finite element formulation, Appl. Numer. Math. 27 (1998) 253-267.
- [7] H. Ji, F. Wang, J. Chen, Z. Li, A new parameter free partially penalized immersed finite element and the optimal convergence analysis, Numer. Math. 150 (2022) 1035–1086.
- [8] L. Mu, X. Zhang, An immersed weak Galerkin method for elliptic interface problems, J. Comput. Appl. Math. 362 (2019) 471-483.
- [9] S. Cao, L. Chen, R. Guo, F. Lin, Immersed virtual element methods for elliptic interface problems in two dimensions, J. Sci. Comput. 93 (2022) 12.
- [10] X. Liu, T. Sideris, Convergence of the ghost fluid method for elliptic equations with interfaces, Math. Comp. 72 (2003) 1731-1746.
- [11] C. Chu, I. Graham, T. Hou, A new multiscale finite element method for high-contrast elliptic interface problems, Math. Comp. 79 (2010) 1915–1955.
- [12] H. Dong, B. Wang, Z. Xie, An unfitted hybridizable discontinuous Galerkin method for the Poisson interface problem and its error analysis, IMA J. Numer. Anal. 37 (2017) 444–476.
- [13] Y. Han, H. Chen, X. Wang, X. Xie, Extended HDG methods for second order elliptic interface problem, J. Sci. Comput. 84 (2020) 22.
- [14] Y. Xiao, J. Xu, F. Wang, High-order extended finite element methods for solving interface problems, Comput. Methods Appl. Mech. Engrg. 364 (2020) 112964.
- [15] P. Cao, J. Chen, F. Wang, An extended mixed finite element method for elliptic interface problems, Comput. Math. Appl. 113 (2022) 148-159.
- [16] A. Hansbo, P. Hansbo, An unfitted finite element method, based on Nitsches method, for elliptic interface problems, Comput. Methods Appl. Mech. Engrg. 191 (2002) 5537–5552.
- [17] E. Burman, S. Claus, P. Hansbo, M. Clarson, A. Massing, CutFEM: Discretizing geometry and partial differential equations, Internat. J. Numer. Methods Engrg. 104 (2015) 472–501.
- [18] L. Huynh, N. Nguyen, J. Peraire, B. Khoo, A high-order hybridizable discontinuous Galerkin method for elliptic interface problems, Internat. J. Numer. Methods Engrg. 93 (2013) 183–200.
- [19] Y. Liu, Y. Wang, Polygonal discontinuous Galerkin methods on curved region and its multigrid preconditioner, Math. Numer. Sin. 44 (2022) 396-421.

- [20] Y. Wang, F. Gao, J. Cui, A conforming discontinuous Galerkin finite element method for elliptic interface problems, J. Comput. Appl. Math. 412 (2022) 114304.
- [21] S. Yu, G. Wei, Three-dimensional matched interface and boundary (MIB) method for treating geometric singularities, J. Comput. Phys. 227 (2007) 602-632.
- [22] Y. Zhou, S. Zhao, M. Feig, G. Wei, High order matched interface and boundary method for elliptic equations with discontinuous coefficients and singular sources, J. Comput. Phys. 213 (2006) 1–30.
- [23] L. Chen, H. Wei, M. Wen, An interface-fitted mesh generator and virtual element methods for elliptic interface problems, J. Comput. Phys. 334 (2017) 327–348.
- [24] L. Mu, J. Wang, G. Wei, X. Ye, S. Zhao, Weak Galerkin methods for second order elliptic interface problems, J. Comput. Phys. 250 (2013) 106-125.
- [25] L. Mu, J. Wang, X. Ye, S. Zhao, A new weak Galerkin finite element method for elliptic interfce problems, J. Comput. Phys. 325 (2016) 157-173.
- [26] C. Wang, S. Zhang, A weak Galerkin method for elasticity interface problems, J. Comput. Appl. Math. 419 (2023) 114726.
- [27] W. Cao, C. Wang, J. Wang, A new primal-dual weak Galerkin method for elliptic interface problems with low regularity assumptions, J. Comput. Phys. 470 (2022) 111538.
- [28] J. Wang, X. Ye, A weak Galerkin finite element method for second-order elliptic problems, J. Comput. Appl. Math. 241 (2013) 103-115.
- [29] D. Li, C. Wang, J. Wang, Generalized weak Galerkin finite element methods for biharmonic equations, J. Comput. Appl. Math. 434 (2023) 115353.
- [30] D. Li, C. Wang, J. Wang, An L^p-primal-dual finite element method for first-order transport problems, J. Comput. Appl. Math. 434 (2023) 115345.
- [31] D. Li, C. Wang, A simplified primal-dual weak Galerkin finite element method for Fokker-Planck type equations, Numer. Methods Partial Differ. Equ. 39 (2023) 3942–3963.
- [32] W. Cao, C. Wang, J. Wang, An L^p-primal-dual weak Galerkin method for convection-diffusion equations, J. Comput. Appl. Math. 419 (2023) 114698.
- [33] S. Cao, C. Wang, J. Wang, A new numerical method for div-curl systems with low regularity assumptions, Comput. Math. Appl. 114 (2022) 47-59.
- [34] C. Wang, J. Wang, X. Ye, S. Zhang, De Rham complexes for weak Galerkin finite element spaces, J. Comput. Appl. Math. 397 (2021) 113645.
- [35] C. Wang, J. Wang, A primal-dual weak Galerkin finite element method for Fokker-Planck type equations, SIAM J. Numer. Anal. 58 (2020) 2632–2661.
- [36] C. Wang, J. Wang, A primal-dual weak Galerkin finite element method for second order elliptic equations in non-divergence form, Math. Comp. 87 (2018) 515-545.
- [37] H. Huang, J. Li, J. Yan, High order symmetric diect discontinuous Galerkin method for elliptic problems with fitted meshes, J. Comput. Phys. 409 (2020) 109301.
- [38] L. Beirão da Veiga, A. Russo, G. Vacca, The virtual element method with curved edges, ESAIM Math. Model. Numer. Anal. 53 (2019) 375-404.
- [39] D. Gilbarg, N. Trudinger, Elliptic Partial Differential Equations of Second Order, second ed., Springer-Verlag, Berlin, 1983.
- [40] J. Wang, X. Ye, A weak Galerkin mixed finite element method for second-order elliptic problems, Math. Comp. 83 (2014) 2101-2126.
- [41] D. Li, C. Wang, J. Wang, Curved elements in weak Galerkin finite element methods, Comput. Math. Appl. 153 (2024) 20-32.
- [42] L. Mu, J. Wang, X. Ye, A weak Galerkin finite element method with polynomial reduction, J. Comput. Appl. Math. 285 (2015) 45-58.